2018-01-0199 Published 03 Apr 2018

Numerical Investigation of Natural Gas-Diesel Dual Fuel Engine with End Gas Ignition

Apoorv Talekar and Ming-Chia Lai Wayne State University

Eiji Tomita and Nobuyuki Kawahara Okayama University

Ke Zeng and Bo Yang Xian Jiaotong University

Citation: Talekar, A., Lai, M.-C., Tomita, E., Kawahara, N. et al., "Numerical Investigation of Natural Gas-Diesel Dual Fuel Engine with End Gas Ignition," SAE Technical Paper 2018-01-0199, 2018, doi:10.4271/2018-01-0199.

Abstract

The present study helps to understand the local combustion characteristics of PREmixed Mixture Ignition in the End-gas Region (PREMIER) combustion mode while using increasing amount of natural gas as a diesel substitute in conventional CI engine. In order to reduce NO_x emission and diesel fuel consumption micro-pilot diesel injection in premixed natural gas-air mixture is a promising technique. New strategy has been employed to simulate dual fuel combustion which uses well established combustion models. Main focus of the simulation is at detection of an end gas ignition, and creating an unified modeling approach for dual fuel combustion. In this study G-equation flame propagation model is used with detailed chemistry in order to detect end-gas ignition in overall low temperature combustion. This combustion simulation model is validated using comparison with experimental data for dual fuel engine.

Introduction

Dual fuel (diesel-CNG, diesel-syngas or diesel-hydrogen) is one of the efficient, clean yet difficult to model combustion phenomena. Dual fuel combustion has both CI and SI characteristics in addition to its own typical behavior, which increases complexity of the combustion process. Traditionally in dual fuel combustion process diesel spray is introduced in a nearly homogeneous mixture of CNG-air or CNG-hydrogen-air. Diesel combustion has been studied for decades and well-established auto-ignition models are available for CFD-kinetic simulations. As first stage of the dual fuel combustion is auto-ignition these models can be applied directly without any change under the assumption that diesel auto-ignition is not affected by the presence of another fuel species such as methane, and traces of ethane, propane and iso-butane. In reality, traces of any gaseous fuel can change ignition delay, temperature of auto-ignition process, duration of first stage ignition and laminar burning velocity. Hence diesel substitution ratio is very important in order to recognize the percentage of energy delivered by diesel fuel.

$$Diesel\ Substitution\ ratio = \frac{LHV_{CH_4} \times m_{CH_4}}{LHV_{CH_4} \times m_{CH_4} + LHV_{Diesel} \times m_{Diesel}} \quad (1)$$

As this ratio increases beyond 95%, authors have found that traditional auto-ignition model which are created for diesel-like fuels do not predict major combustion phases. Diesel substitution up to 98-99% can be achieved [1] and is desirable. Hence flame propagation model needs to be added and/or used with current auto-ignition model to predict CI and SI characteristics of dual fuel engine. Yang et al. [2, 3, 4] investigated the optimum settings for the natural gas injection under low load for dual fuel engine to improve thermal efficiency. Talekar et al. [5] used G-equation flame propagation model with auto-ignition and detailed kinetic model to simulate dual fuel combustion in different types of engines.

In this study authors have used laminar burning velocity for methane calculated by Gulder's equation [6] which provides correct values for equivalence ratio in the range of 0.5-0.6. As

FIGURE 1 Laminar flame speed (methane) comparison Gulder's vs 1D calculations at 1000 K for methane

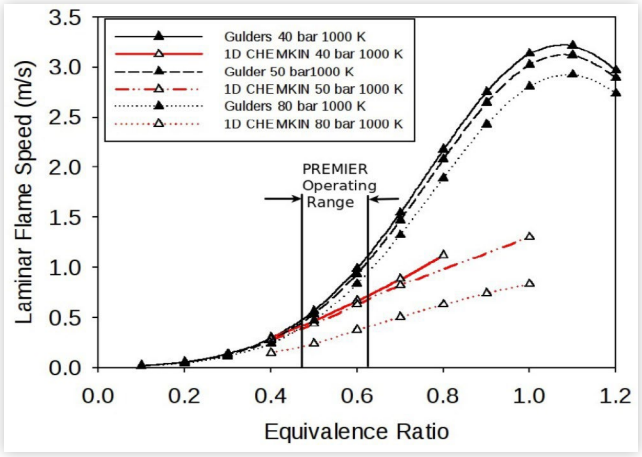

an equivalence ratio differs from 0.6 towards stoichiometric, laminar flame speed calculated using Gulder's equation is higher than experimentally found values as well as values obtained from 1 D simulations. Laminar flame speed is intrinsic property of fuel and hence get affected by traces of other fuel species and stratification [7]. Larger hydrocarbon fuel (such as n-heptane) show reduction in laminar flame speed at phi = 1.5 where as methane shows increase in flame speed at all equivalence ration in between 0.6-1.4 in case of stratification [8]. In the present work author have used corrected laminar flame speed based on 1 D calculations using CHEMKIN and A-SRUF [9]in order to minimize errors arising from initial kernel growth.

As shown in Figure 2 laminar flame speed for methane decreases with increase in initial pressure and increases with higher initial temperature [10]. For higher pressure than 1 MPa, for methane there is hardly any experimental data available for laminar flame speed. Hence it is calculated using 1D numerical simulation for chemical mechanism created for dual fuel operation and is discussed in further section. It is important to note that increasing pressure has diminishing effect on laminar flame speed compared to temperature.

Unified Strategy for Numerical Modeling of Dual Fuel Engines

One of the current challenges in the 3 D CFD simulation of the dual fuel is to get correct heat release from the chemical reactions compared with the experimental data. This is important to predict knock in the dual fuel operation. PREMIER dual fuel combustion [11] mode consists of three stages. In the first stage due to the pilot fuel injection initial flame kernel starts, surrounding the spray evaporation zone and grows into flame. In the second stage flame propagation increases pressure and temperature in the end gas region. In the third and most important phase autoignition of the remaining fuel mixture in the end gas region produces rapid heat release.

FIGURE 2 Laminar flame speed for methane at elevated pressures

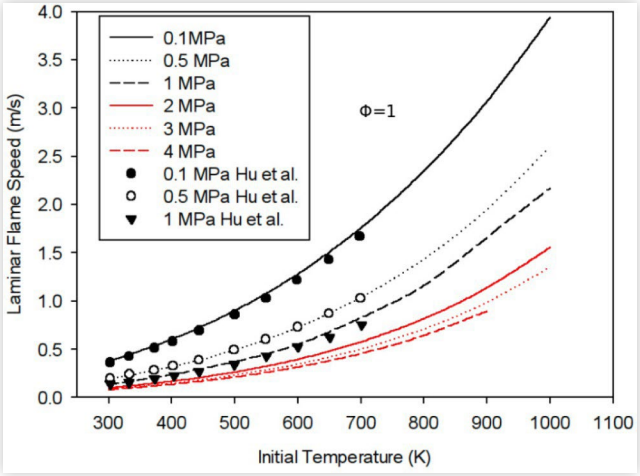

Aksu et al. [12] investigated experimentally the effect of varying concentration of hydrogen on the dual fuel PREMIER combustion. Experimental data showed that the early injection (before 12 BTDC) push regular dual fuel combustion mode to end gas ignition mode and if the H_2 mole fraction in the gaseous fuel is more than 50% then combustion rapidly switches to knocking region. In the recent study by Aksu et al. [1] showed that the spit pilot injection in PREMIER dual fuel mode increases thermal efficiency, IMEP and stabilizes end gas ignition by increasing ignition probability which leads to suppressed knock. Still there is a probability of second injection flame kernel growth occurrence near injector tip depending on the relative time gap between injections and initial kernel growth rate from fist injection.

Dual fuel engine starts combustion using pilot fuel spray and auto-ignition of that small fuel acts as a spark energy for the lean gaseous fuel-air mixture. This mode of combustion can be investigated experimentally, but poses a very complicated problem for 3 D CFD modeling. In SI engines spark location is known and has precise spark energy, spark efficiency and duration of the spark associated with it whereas dual fuel engine heavily depends on the nature of the pilot spray to start premixed flame type combustion.

We have devised a new unified modeling strategy for dual fuel combustion using well established models and its integration. This strategy is at the core of this paper and is explained in depth in following sections.

Numerical Modeling Setup

The sequence of different types of combustion is very important for dual fuel operation mode. For regular dual fuel operation diesel pilot spray evaporate, mix with already almost homogeneous mixture of natural gas and air. During this process, auto-ignition of diesel takes place and produces first heat release. This rate of heat release heavily depends on the quantity of diesel, compression ratio and local equivalence ratio. First ignition starts the flame propagation and consumes most of the gaseous fuel. In this paper authors have focused on the end gas ignition which follows the traditional flame propagation and has significant heat release rate compared to the first two zones, namely auto-ignition of diesel and flame front propagation in lean natural gas- air mixture. Hence auto-ignition model with detailed chemistry and well established flame propagation model hereafter mentioned as G-equation model are used in this paper.

G-Equation Model:

$$\frac{\partial \rho G}{\partial t} + \frac{\partial \rho \widehat{u_i} G}{\partial x_i} = -D_t \kappa \left| \frac{\partial G}{\partial x_i} \right| + \rho_u S_t \left| \frac{\partial G}{\partial x_i} \right| \qquad (2)$$

where D_t is turbulent diffusion, κ is curvature of the flame, ρ_u is unburnt density and S_t is turbulent flame speed.

Depending on the fuel composition and local equivalence ratio ignition temperature found to vary between 950 K - 1100 K and hereafter it is denoted by T_G. This temperature (T_G) was decided using 0 D auto-ignition model for homogeneous charge in CHEMKIN as shown in Figure 3. T_G changes per local

equivalence ratio and fuel composition. For this numerical calculation, 99% diesel substitution ratio for different overall equivalence ratio. Merhubi et al. [13]conducted high pressure (40 bar) methane auto-ignition using shock tube and also validated GRI 3.0 mechanism for phi = 0.5-1.0. At 40 bar pressure auto-ignition temperature of methane (ϕ = 0.5) is 1560 K. Though HCCI calculations assumes premixed charge, it is important to note that 1% diesel quantity by energy content significantly changes auto-ignition temperature of methane. If n-heptane mass fraction is less than 0.021 then T_G is on the higher side. Hence value of T_G needs to be determined each time when the fuel composition changes.

S_t is derived from laminar flame speed S_l, when used for RANS modeling it includes u' root mean square of turbulent fluctuation velocity as shown in equation 3. [14]

$$S_t = S_l + u'\left(\left(\frac{-a_4 b_3^2}{2b_1} D_a\right) + \left[\left(\frac{-a_4 b_3^2}{2b_1} D_a\right)^2 + a_4 b_3^2 D_a\right]^{\frac{1}{2}}\right) \quad (3)$$

where $b_1 = 2.0$, $b_3 = 1.0$ and $a_4 = 0.78$.

Equation 4 derived by Pitsch [15] is used for LES cases to calculate S_t.

$$S_t = S_l\left(\frac{-b_3^2 C_S}{2b_1 S_c}\frac{\Delta}{l_F} + \sqrt{\left(\frac{b_3^2 C_S}{2b_1 S_c}\frac{\Delta}{l_F}\right)^2 + \frac{b_3^2 D_t}{S_l l_F}} + 1\right) \quad (4)$$

where Sc is turbulent Schmidt number, Δ is the filter width and C_s is dynamic Smagorinsky number.

In G-equation model G(x,t) is a non-reactive scalar iso-surface for any fixed value of x. The flame front is described by G = 0 surface and the flame thickness is superimposed by G' on this iso-surface. G-equation depends on the closure solution for calculating turbulent flame speed, and does not have a source term hence G-equation model can be easily coupled with detailed chemistry model [16, 17, 18, 19].

Positive value of G suggests burnt zone and negative value is used for unburnt zone. In the current model laminar flame speed is calculated using CHEMKIN 1 D laminar flame speed calculations instead of Gulder's equation [6] as it tends to over predict the laminar flame speed for single component fuels like methane for high pressure and temperature conditions. As shown in Figure 1 for limited range of equivalence ratio 0.5-0.6 and 1.5 laminar flame speed prediction using Gulder's equation is correct compared to the 1 D flamespeed calculated using GRI 3.0 mechanism [20]. The implementation of G-equation model heavily depends on the laminar flame speed and the turbulent velocity, hence choice of correct turbulent model and accurate flame speed are important for overall reliability of the modeling strategy.

FIGURE 3 Ignition temperature for different equivalence ratio

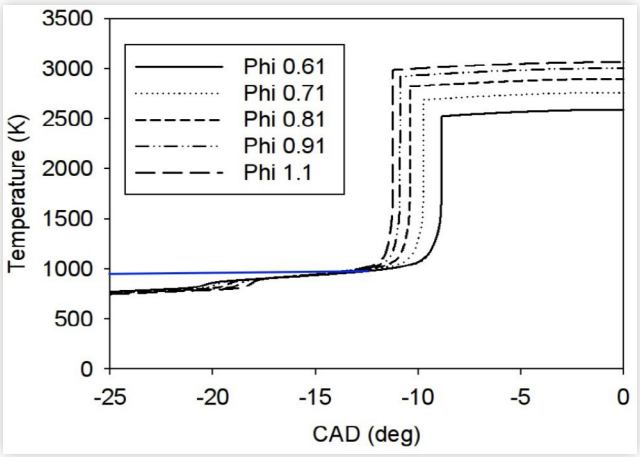

Chemical Mechanism for Dual Fuel Combustion Mode

N-heptane detailed mechanism hereafter called LLNL detailed mechanism [21] and GRI 3.0 (53 species and 325 reactions) [20] mechanisms are used to create a new reduced mechanism for the dual fuel operation using CHEMKIN software. C_3-C_8 reactions from LLNL detailed mechanism are retained and C_1-C_2 reactions with NO_x mechanism are added from GRI 3.0 mechanism. In dual fuel mode, combustion process starts with autoignition of atomized diesel and in turn acts as source of energy like spark for methane ignition. Autoignition temperature of methane is much higher than diesel hence rate of heat release can be controlled by varying diesel injection quantity and timing. Multizone HCCI 0 D simulation was used to create this mechanism and the results were compared with the experimental data from the literature. To account for the heat lost convective heat transfer coefficient was added for every wall of the combustion chamber [22]. The combustion volume was divided into 7 parts depending on the temperature range and the equivalence ratio. These volumes are assumed to not exchange mass but only energy during the simulation. Intermediate chemical mechanism obtained consisted of 181 species and 1714 reactions. Dual fuel combustion is more sensitive towards low temperature combustion, hence few more 0 D simulations were performed to check the integrity of the new mechanism against literature data, especially for different values of exhaust gas recirculation (EGR). Still 1714 reactions are computationally expensive to run 3D combustion simulations hence more reduction was necessary without losing the low temperature chemical pathways. Direct relation graph with error propagation (DRGEP) is well established method for the mechanism reduction but for better results needs to be coupled with extensive sensitivity analysis. Also DRGEP only considers only strongest reaction paths in case of parallel pathways with more than one species in common. Path flux analysis (PFA) method [23, 24, 25] has proven to be less time consuming with better results. Hence PFA method is used to reduce mechanism further.

Initiation of Burnt Zone after Auto-Ignition

From the start of the simulation, G value is set to arbitrary −0.1constant value which shows unburnt zone for entire combustion chamber volume. Depending on the fuel

composition and local equivalence ratio ignition temperature found to vary between 950 K - 1100 K hereafter denoted by T_G. This temperature (T_G) was decided using 0 D auto-ignition model for homogeneous charge in CHEMKIN for the compression ratio 17:1 as shown in Figure 3. T_G changes as per local equivalence ratio and fuel composition. For this numerical calculation, 99% diesel substitution ratio is used for different overall equivalence ratios. Merhubi et al. [13] conducted high pressure (40 bar) methane auto-ignition using shock tube and also validated GRI 3.0 mechanism for ϕ =0.5-1.0. At 40 bar pressure auto-ignition temperature of methane (ϕ = 0.5) is 1560 K. Though HCCI calculations assumes premixed charge, it is important to note that 1% diesel quantity by energy content significantly changes auto-ignition temperature of methane. If n-heptane mass fraction is less than 0.021 then T_G is on the higher side. Hence value of T_G needs to be determined each time when the fuel composition changes.

When used alone G-equation model, we rely on the flame propagation progress to calculate heat release. This calculation over-simplifies the combustion progress by assuming chemical and thermal equilibrium at the flame surface and accounts simplifies the combustion progress by assuming chemical and thermal equilibrium at the flame surface and accounts for sudden density change form unburnt mixture to bunt species mixture. Time dependent and slow mechanisms like NO_x formation can not be implemented correctly due to high temperature of flame surface, which can result in high production of NO_x species. But when G-equation is coupled with the detailed chemistry model, heat release depends on the chemical reactions and hence pollutant formation can be predicted with relatively better accuracy. In this paper authors intend to discuss the effect of flame modeling with detailed chemistry and its necessity in the dual fuel simulation. Also integration of G-equation with LES turbulent model is robust and provides very detailed flame front location staring with spray as kernels and also detects high temperature regions in the end gas region [26, 15].

In Figure 4 experimental images of flame kernel are asymmetric and can only be achieved by modeling entire combustion chamber instead of sector mesh.

Engine Specifications

TABLE 1 PREMIER dual fuel engine specifications

Item	PREMIER
Engine Type	4-stroke
Cylinder number	4 (deep-dish)
Bore X stroke	98 mm x 108 mm
Compression ratio	17.0: 1
Injection system	DI
Max. injection pressure	40, 80 MPa
Injection nozzle	3 x 0.1 mm
Engine Speed (rpm)	1000

Spray Modeling

Spray modeling decides the initial ignition sites for auto-ignition and these sites serve as a initial kernel growth zones for the flame propagation model. Figure 4 validates the kernel growth prediction for single fuel combustion using n-heptane as PRF and experimental [1] images of split micro injection initial kernel development. Combustion chamber without valves is modeled and is discussed in the geometry section in detailed. KH-RT spray model was used instead of TAB spray model. 20000 parcels per nozzle were introduced in the combustion chamber with solid cone structure instead of hollow cone spray. Number of child parcels/droplets created due to the breakup model were limited to maximum

FIGURE 4 Kernel growth comparison with experimental images for Case 4 without natural gas

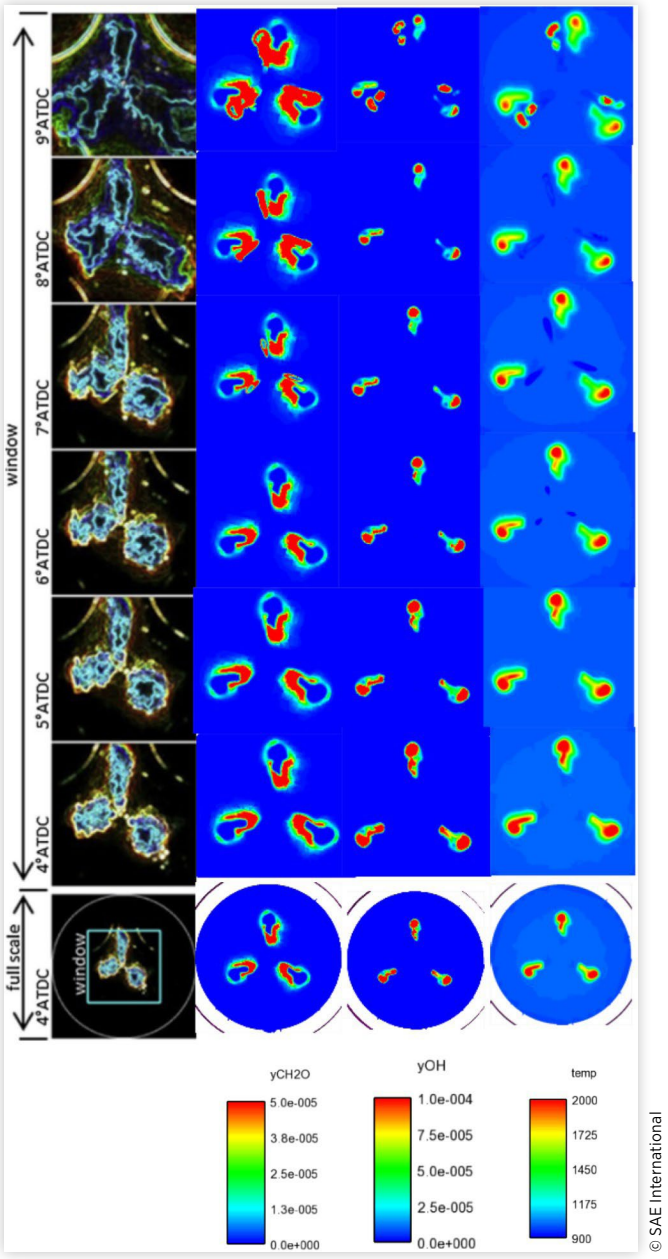

1.5 million. Coefficient of discharge (C_d) is kept constant to 0.85 for all nozzles. Spray was injected (at 40 MPa) in a premixed mixture of methane and air of equivalence ratio 05, 0.6 and 0.8. PREMIER dual fuel combustion cases has 3 nozzle injector.

Geometry and Mesh

A full combustion chamber with initial 100 K cells were used to avoid oversimplified combustion domain. In case of sector mesh symmetrical boundary condition produces mirror images of the 3 D domain between two spray jets. In reality this is not the case and combustion is asymmetric in nature as shown by the experimental images (Figure 4) of flame kernel by Aksu et al. [1]. It is also important to note that symmetry boundary condition on the sector mesh does not justify for inter-jet mixing. Hence full combustion chamber was used with deep dish shape for PREMIER combustion.

Automatic mesh refinement based on the unresolved temperature gradient, species concentration and local flame front has been used. Maximum number of cells were limited to 1.2 million because of the limitations of computational time and resources.

Case Matrix

TABLE 2 PREMIER dual fuel cases

Case No.	SOI (ATDC)	RPM	Max Inj P (MPa)	Diesel Sub%	CH_4 (mg/cyl.)	Diesel inj./cyl. (mg)	λ	IMEP (MPa)	η %
1	−4.5	1000	40	83.21	12	3	1.66	1.11	40
2	−2.5	1000	80	83.21	12	3	1.66	1.20	40
3	−14.5	1000	40	96	25	0.8	1.92	1.50	42
4	−6 & 5	1000	40	98.95	26.7	0.3, 0.3	1.66	0.82	48

Comparison of Simulation and Experimental Data

Figure 5 and 6 show comparison of simulation data with experimental pressure for 95% diesel substitution rate. Difference in injection pressure and later injection timing is cause of late heat release in case 2. As mentioned earlier, higher diesel substitution ratio i.e. lower injection mass of n-heptane (diesel surrogate) create less number of ignition sites in the dual fuel operation. It is important to capture these ignition sites in order to start flame propagation at multiple locations. In cases 3 diesel substitution rate is 96% with single injection of diesel pilot (0.8 mg) where as in case 4 diesel pilot quantity is much smaller (0.6 mg total) and it is split into two micro-pilots pushing diesel substitution to the highest 98.95%.

Discussion

Figure 10 shows combustion progress 10 CA after injection has occurred at 14.5 ATDC for case 3. CH_2O is main attribute

FIGURE 5 SOI 4.5 BTDC case 1

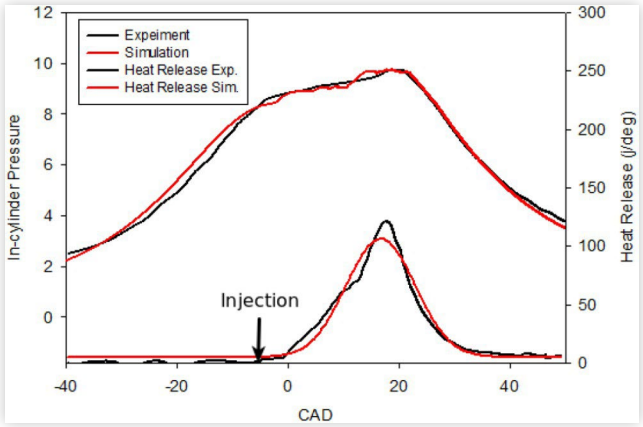

FIGURE 6 SOI 2.5 BTDC case 2

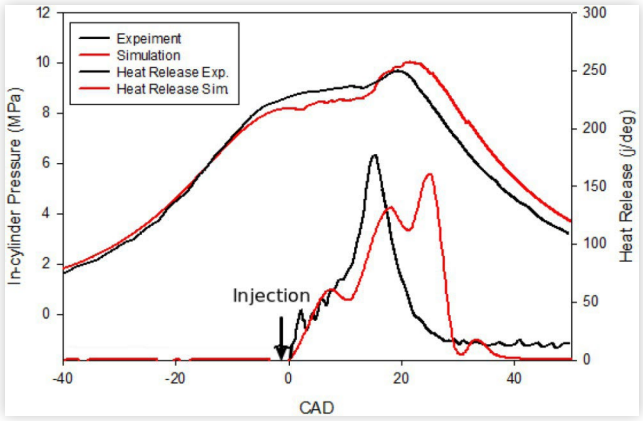

FIGURE 7 Pressure comparison between LES and RANS simulations for case 3

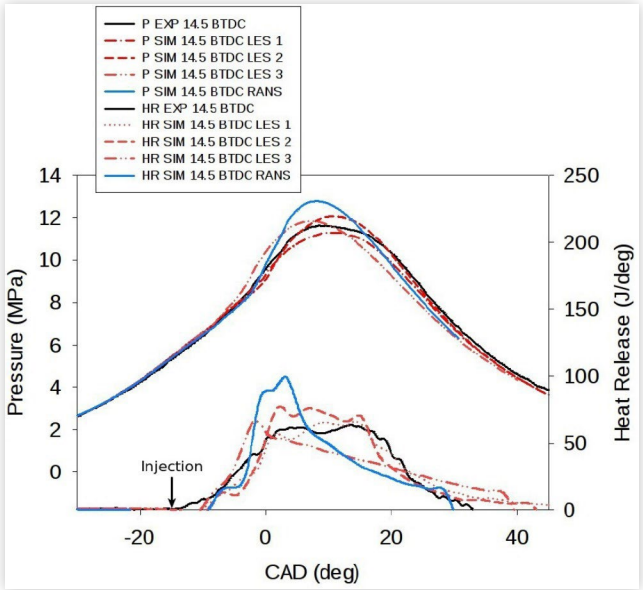

FIGURE 8 SOI 6 BTDC 5 ATDC pressure for continuous LES runs for case 4

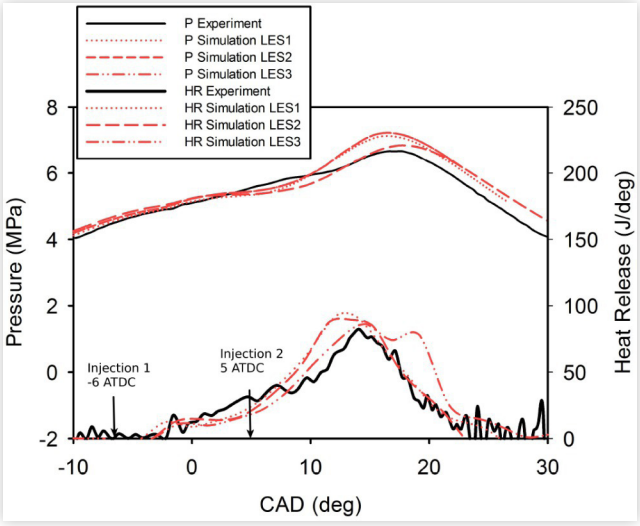

FIGURE 9 Start of end-gas auto-ignition in RANS PREMIER Simulation case 3

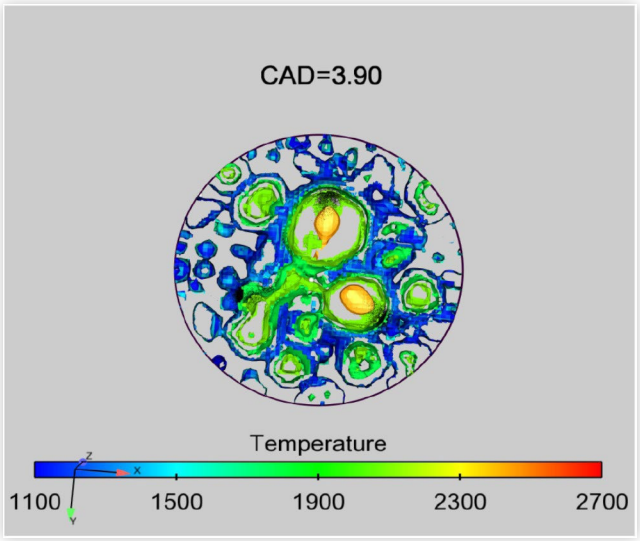

FIGURE 10 CH_2O, G iso-surfaces for low-temperature flame localization and OH for high-temperature combustion for case 3 (–14.5 ATDC inj) run 2

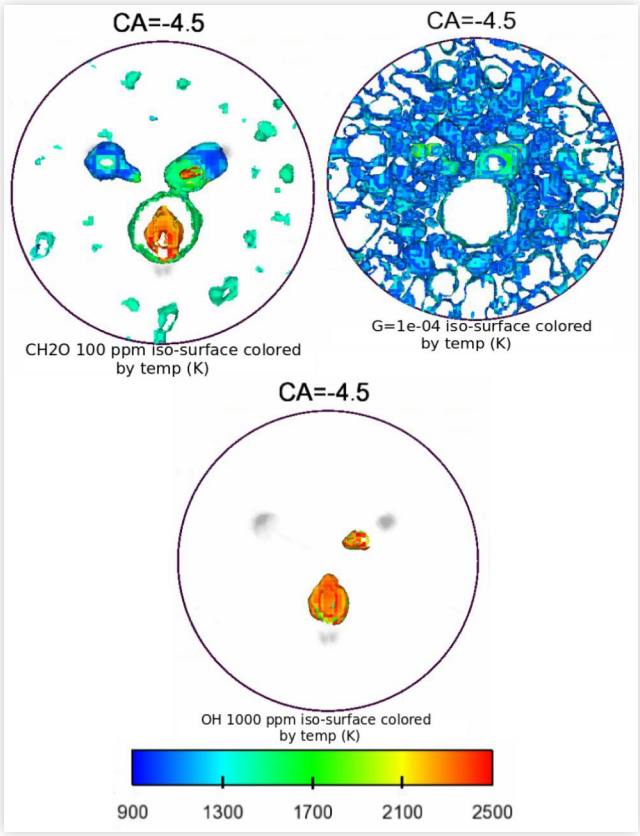

of low temperature combustion appears not only in the vicinity of the flame kernels but on the peripheral area of entire combustion chamber. For the same CA when G = 0.0001 iso-surface is plotted, it shows predominantly low-temperature regions. The empty region in the middle of combustion chamber is high temperature zone and in the third figure, OH concentration is highest in the same region. This shows the smaller hight temperature region near spray surrounded by cluster of low-temperature ignition sites.

Heat release in case of the split micro-pilot injection is illustrated with CH_2O and G iso-surface shown in Figure 11 at 6 ATDC. In case 4, first micro-pilot injection occurs at 6 BTDC and Figure 11 captures the aftermath for flame kernel development after second micro-pilot injection at 5 ATDC. Positive value of G suggest burnt region and negative value shows the unburnt outside the flame zone where as G = 0 is the mean flame front brush. CH_2O and G-surfaces are colored by temperature to show low-temperature flame segments. G = 1e-04 shows the 0.1 mm zone inside the burnt zone after flame front has passed. CH_2O iso-surface shows in the pre-flame chemistry occurring outside the flame front at much lower temperature of 900 K, where inside the burnt zone temperature is much higher 2500 K.

Taylor micro-scale is resolved to 1 mm for the G = 0 flame surface is LES modeling. Number of flame kernel which initiate at the site of high temperature auto-ignition is limited to 50 in both RANS and LES modeling. It was found by trial and error method that if higher number of kernels were used then the fuel consumption rate increases drastically and provides higher rate of heat release in return. Figure 7 shows an in-cylinder pressure for LES turbulence model is over-predicted compared to RANS turbulence model for case 4. Figure 11 shows the development of the initial kernel for case 4 after the second micro-pilot injection is complete. CH_2O iso-surface is created for highest concentration and colored by temperature to show the sites of pre-ignition low-temperature chemistry. Subsequently G iso-surface at value 1e-04 i.e. at 0.1 mm distance form mean flame front inside the burn zone is also colored by temperature shows three major kernel formation zones around three spray lobes. It is very important to note that outside the flame zone, at low temperature initial kernel development starts

FIGURE 11 CH_2O, G iso-surfaces for low-temperature flame localization and OH for high-temperature combustion for case 4 (6 BTDC, 5 ATDC inj) run 2

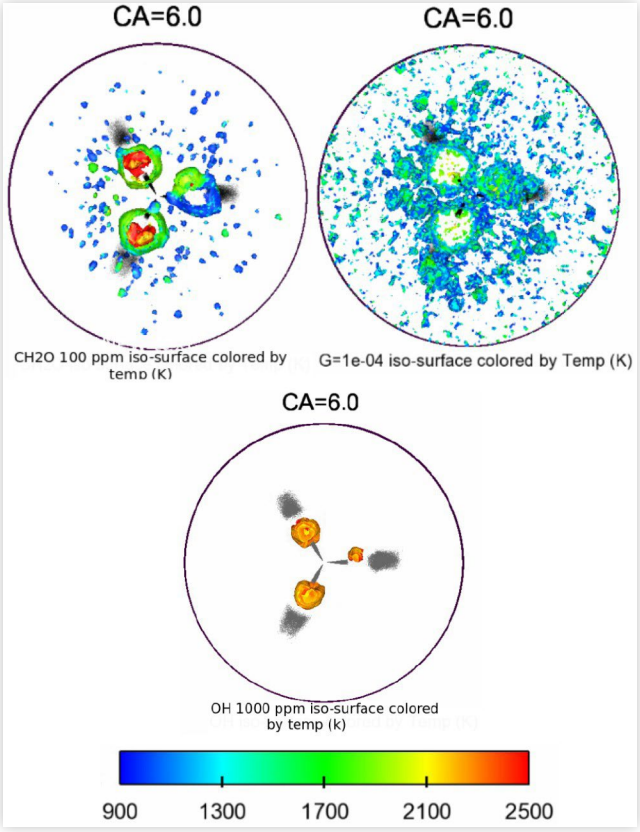

at various locations. These kernel depending on the location from the wall and from mean flame front either become auto-ignition sites or just contribute to small energy release. OH iso-surface is plotted at highest mass fraction of OH (1.e-03) shows the high temperature chemistry inside the burnt zone.

As shown Figure 4 kernel growth for split injection event for case 4 is compared with the experimental images obtained by Aksu et al. [1] only for diesel mode of operation. New simulation was run for this visual comparison. Without G-equation this new simulation ran for 72 hours on 32 CPU cores (only till initial kernel development) which proved to be twice as much slower compared to G-equation with detailed chemistry model for entire cycle. Kernel images show major part is composed of CH_2O and HCO* radicals. Associated temperature range confirm the low-temperature flame also investigated by Zha et al. [27]. Some of the invisible part of the kernel tip at 8 ATDC and 9 ATDC show high temperature combustion region and is highly associated with OH radical. Area of high temperature region in flame kernel is very small compared to the area of low temperature region and CH_2O concentration. Overall surrounding area of the flame kernel (temperature range 970 K - 1000 K) act as a ignition source for lean methane-air mixture. As per the author's knowledge there has not been confirmed studies to experimentally observe change in flame speed from diffusive to premixed flame i.e. from initial kernel to stable premixed flame. There supposed to be an upward jump in flame speed and needs to be determined separately for laminar cases which is outside the focus of this paper but is considered as future work.

Figure 12 shows trend of local temperature for case 3 which include single micro pilot injection at 14.5 BTDC. Highest temperature is noted from pre-heat region (1 mm away from the flame front) and second highest temperature belongs to the burnt region (1-2 mm inside the flame front). It is also important to note that around 6 BTDC mean flame front (G = 0) reaches highest temperature and at the same time in pre-heat region 2-5 mm away from mean flame) there is sudden increase in temperature. This is a very clear indication of end-gas ignition provided that temperature is much less at 0.5 mm outside the flame. In Figure 13 show the local temperature and pressure data for the same scenario and there are two major heat release zones first one is at 1000 K range and second zone shows high temperature end gas heat release at 2100 K range. Both LES and RANS turbulent models with

FIGURE 12 Temperature profile for different G values for case 3

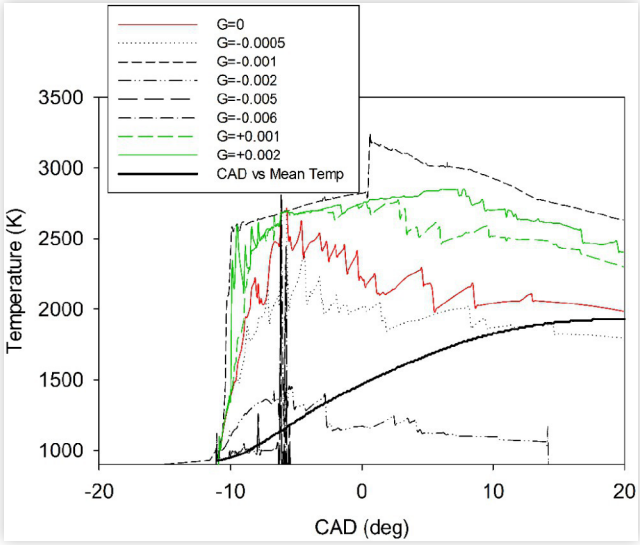

FIGURE 13 Local temperature vs pressure for case 3

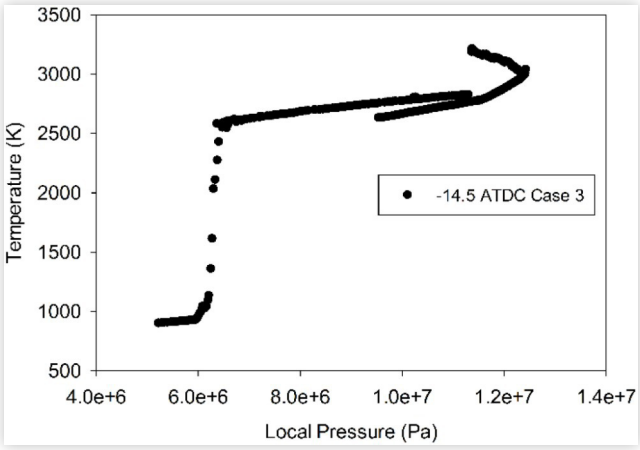

same combustion model show good agreement in terms of end gas ignition.

The pressure drop after TDC for both LES and RANS is comparable. G = 0 surface is colored by temperature which shows 1100 K and the inner zones show G > 0 value for burnt zone where temperature reaches maximum after pilot auto-ignition and has distinct three lobes for respective nozzle sprays.

Compared to Figure 13 for local temperature vs local pressure Figure 15 shows much clear trend. This is due to the effect of split micro-pilot injection. For case 3 has a single pilot injection of mass 2.6 times each split pilot injected mass of case 4. For case 3 maximum temperature occurrence belongs to the pre-flame region (G = −0.001) and end-gas ignition where as for case 4 maximum temperature occurs in the post-flame burnt region. Ignition sites for split pilot case 4 are less in number compared to the early injection (14.5 BTDC) of single pilot of case 3, indirectly controlling the end-gas ignition. Figure 15 shows the effect of methane on the first ignition temperature as well as the overall temperature trend. For case 4 when methane is present first stage ignition temperature is lower as compared to the scenario when methane is not present. On the contrary at second stage ignition methane burns at higher temperature compared to diesel only case (Figure 4). As the second micro-pilot starts at 5 ATDC for non-methane case temperature suddenly drops as spray is being injected in the developed flame kernel of the first pilot injection. Start of the second micro-pilot is visible in Figure 11. This effect is reduced in case 4 due to presence of methane and flame kernel grows with steady consumption of fuel. Split injection proves to be effective in controlling end gas ignition and growth of the flame kernel. Current way of modeling proved to be very effective in detecting changes in the end-gas ignition temperature as well as its precise location and frequency evident from Figure 9-11.

FIGURE 14 Temperature profiles for different G values for case 4

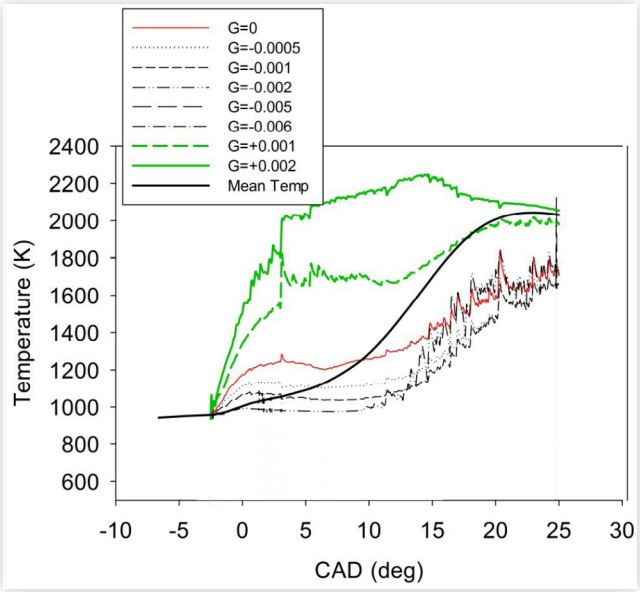

FIGURE 15 Local temperature vs pressure for case 4 with and without methane/CNG

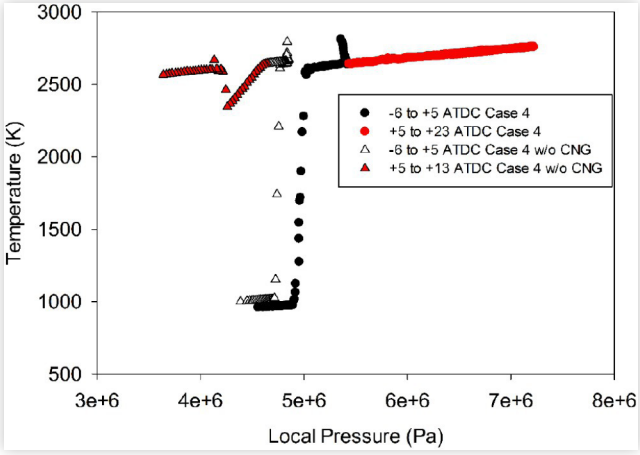

Numerical modeling of the dual fuel involves transitioning from auto-ignition to flame propagation and in case of PREMIER combustion there is additional end-gas auto-ignition. These transitions makes dual fuel combustion simulation more intricate and difficult to predict. For the correct modeling of PREMIER combustion mode, all auto-ignition sites needs to be captured and should be considered the starting points of the premixed turbulent deflagrative flame which causes end-gas ignition. Detailed chemistry model used for regular CI diesel (n-heptane as surrogate fuel) auto-ignition process shows the rate of fuel consumption is higher compared to the premixed flame propagation. As the spray atomizes in the air-methane mixture, it forms locally premixed site for n-heptane+methane/air. This mixture when auto-ignited gives rise to the small kernel formation and G = 0 surface gets created at that site. The propagation after initial kernel development of this flame front heavily depends on the laminar flame speed of the fuel mixture. Spray kernel which is locally fuel rich is in contact with lean air-fuel mixture, this fuel gradient drastically changes the laminar flame speed. More recently Shi et al. [7,8] found that stratified methane/air laminar flame speed shows stronger enhancement over homogeneous lean methane/air mixture using 1D simulation while showing less fuel consumption rate compared with the homogeneous mixture. In 3D modeling to resolve the gradient between homogeneous and stratified charge more precise LES modeling with high density mesh is necessary which is computationally expensive. Gradient of G represents the temperature profiles in three combustion regions as shown in Figure 14, positive values of G represent the temperature in the burnt zone where post flame chemistry is dominant and has highest temperature in the combustion chamber. Negative values of G shows the pre-heat or pre-flame regime where end-gas ignition happens in PREMIER cases. This is excellent way of predicting temperature in end-gas region instead of just observing few locations for higher heat release. Monitoring the end-gas region for temperature spikes is easier by tracking gradient values of G and also provides much larger data set compared to traditional way of monitoring few points in combustion chamber space. As the flame

progresses into the combustion chamber the temperature profile of G = 0 and G < 0 vales become more irregular, which is a prominent indication of end-gas heat release. G equation resolves the turbulent flame propagation. Kernels of this G-equation model can start different flame fronts at different locations. The criteria for the start of the flame front is user defined and it is 970 K for PREMIER combustion. Any cell in the combustion chamber when reaches to the 970 K, G-equation starts to locate flame surface designed by scalar G = 0. Before this incidence global G value is set to be −0.1. Due to flame propagation model rate of heat release from the autoignition zone around the spray evaporation zone is reduced [5]. Turbulent flame speed is highly dependent on the mesh size and velocity gradient. For all the simulation wall temperature was initialized from a constant value which might deviate from the experimental conditions. Though Figure 5-8 show good comparison and agreement between experimental and simulation pressure trace for traditional dual fuel operation, numerical results over predict pressure in premixed region. This is due to mesh dependence of G-equation as optimization of the G-equation coefficient is proven to be difficult. New numerical method should be created for handling auto-ignition (high temperature gradient zone and staring point for premixed flame) and G' variable surface together. In the current numerical setup G equation divides combustion chamber into three volumes, unburnt region, burnt region and flame thickness. Flame thickness is considered at chemical equilibrium and is determined by turbulent flame speed and G'. Flame thickness range in between 0.1-0.5 mm.

Detailed chemistry modeling and flame propagation both are advance modeling strategies, but when used alone may not be adequate to model dual fuel engine which has CI and SI characteristics. The end-gas ignition contours of the ignition zones show that number of ignition sites are more for the flame propagation model.

In Figure 7 & 8 simulation predicted pressure shows good agreement with the experimental data [1,12]. Due to the initial kernel size (Figure 4) the rate of fuel consumption can change for different injection timing. Split micro pilot can be used to reduce knocking to certain level to obtain PREMIER characteristics. Initial flame kernel growth plays very important role in this case. If the second injection occurs after the first kernel growth is complete then final kernel growth is restricted. Also split pilot increases thermal efficiency efficiency by converting normal combustion mode to PREMIER while using less diesel fuel in process hence increasing diesel substitution ratio to the highest possible value of 98.95%.

Conclusion

Flame propagation model increases difficulty level, complexity and computational time of the simulation but provides important insight to the dual fuel combustion modeling. Initial kernel growth, flame propagation, spacial knock detection and interaction between spray and flame surface can be studies in detail using the new unified dual fuel modeling strategy. As this model uses detailed chemistry inside and outside of the flame zone, knock detection is most dominant feature of this model. End-gas ignition and heat release from hot spots in dual fuel operation can be easily identified without using any extensive post-processing for concentration profiles of the chemical species. Same strategy can be used in RANS and LES turbulence modeling. Interaction of the flame surface and the pre-flame region needs to be studied in detail to understand overall low temperature combustion with end-gas ignition. In addition to this few more conclusion can be drawn from this study:

1. Extreme diesel substitution ratio of 96-99% at low load in dual fuel mode promotes end-gas ignition and is controllable. Although very difficult to capture just using detailed chemistry, when used with G-equation proved to be quite effective to detect end-gas ignition in both RANS and LES modeling.
2. Using G-equation with detailed chemistry proved to be computationally efficient compared to traditional detailed chemistry model.
3. G-equation model is heavily dependent on the laminar flame speed. For single fuel such as methane determination of laminar flame speed is relatively easy and well established by literature. But for dual-fuel start of the flame propagation is affected by presence of heavy molecules and needs to be considered while making corrections to the laminar flame speed.
4. Gulder's flame speed correlation can be used at certain range of equivalence ratio. For stoichiometric mixtures, Gulder's correction tend to over-predict the laminar flame speed and should be accounted for in combustion model.
5. Small traces of methane changes auto-ignition behavior of n-heptane. Two distinct temperature regions were detected for start of ignition and end-gas auto-ignition. Low temperature combustion at the initial stages of the kernel development delays the major heat release which accompanies the end-gas ignition at later stages.
6. Pre-flame chemistry plays vital role in end-gas ignition and is well captured by the G-equation and detailed chemistry modeling. Although micro-pilot spray pressure has significant effect on the initial kernel growth, better results can be obtained with higher number of initial parcels and KH-RT spray model with correct needle profile.
7. Overall new unified combustion model proved to effective to predict most extreme dual fuel combustion mode including three major intertwined processes of slow kernel development, flame propagation and end-gas ignition.

References

1. Aksu, C., Kawahara, N., Tsuboi, K., Kondo, M. et al., "Extension of PREMIER Combustion Operation Range Using Split Micro Pilot Fuel Injection in a Dual Fuel Natural

Gas Compression Ignition Engine : A Performance-Based and Visual Investigation," *Fuel* 185:243-253, 2016, doi:10.1016/j.fuel.2016.07.120.

2. Yang, B., Wei, X., Xi, C., Liu, Y. et al., "Parametric Investigation of Natural Gas Port Injection and Diesel Pilot Injection on the Combustion and Emissions of a Turbocharged Common Rail Dual-Fuel Engine at Low Load," *ENERGY Convers. Manag.* 87:297-304, 2014, doi:10.1016/j.enconman.2014.07.030.
3. Yang, B., Wei, X., Xi, C., Liu, Y. et al., "Experimental Study of the Effects of Natural Gas Injection Timing on the Combustion Performance and Emissions of a Turbocharged Common Rail Dual-Fuel Engine," *Energy Convers. Manag.* 87:297-304, 2014, doi:10.1016/j.enconman.2014.07.030.
4. Yang, B., Wei, X., and Zeng, K., "The Development of an Electronic Control Unit for a High Pressure Common Rail Diesel/Natural Gas Dual-Fuel Engine," SAE Technical Paper 2014-01-1168, 2014, doi:10.4271/2014-01-1168.
5. Talekar, A.P., Lai, M., Zeng, K., and Yang, B., "Simulation of Dual-Fuel-CI and Single-Fuel-SI Engine Combustion Fueled with CNG," *SAE Technical Papor 2016-01-0789*, 2016, doi:10.4271/2016-01-0789.
6. Gulder, O.L., "Correlations of Laminar Combustion Data for Alternative S.I. Engine Fuels," SAE Technical Paper 841000, 1984, doi:10.4271/841000.
7. Shi, X., Chen, J., and Chen, Z., "Numerical Study of Laminar Flame Speed of Fuel-Stratified Hydrogen/Air Flames," *Combustion and Flame* 163:394-405, 2016, doi:10.1016/j.combustflame.2015.10.014.
8. Shi, X., Chen, J., and Chen, Y., "Laminar Flame Speeds of Stratified Methane, Propane, and n-Heptane Flames," *Combustion and Flame* 176:38-47, 2017, doi:10.1016/j.combustflame.2016.10.018.
9. Chen, Z., "*Studies on the Initiation, Propagation, and Extinction of Premixed Flames*," (Princeton University, 2008).
10. Hu, E., Li, X., Meng, X., Chen, Y. et al., "Laminar Flame Speeds and Ignition Delay Times of Methane-Air Mixtures at Elevated Temperatures and Pressures," *Fuel* 158:1-10, 2015, doi:10.1016/j.fuel.2015.05.010.
11. Azimov, U., Tomita, E., and Kawahara, N., "Ignition, Combustion and Exhaust Emission Characteristics of Micro-Pilot Ignited Dual-Fuel Engine Operated under PREMIER Combustion Mode," 2011.
12. Aksu, C., Kawahara, N., Tsuboi, K., Nanba, S. et al., "Effect of Hydrogen Concentration on Engine Performance, Exhaust Emissions and Operation Range of PREMIER Combustion in a Dual Fuel Gas Engine Using Methane-Hydrogen Mixtures," *JSAE* 20159, 2015.
13. El Merhubi, H., Kéromnès, A., Catalano, G., Lefort, B. et al., "A High Pressure Experimental and Numerical Study of Methane Ignition," *Fuel* 177:164-172, 2016, doi:10.1016/j.fuel.2016.03.016.
14. Peters, N., "*Turbulent Combustion*," (Cambridge University Press), ISBN 9780521660822.
15. Pitsch, B.H., "A G-Equation Formulation for Large-Eddy Simulation of Premixed Turbulent Combustion," *Cent. Turbul. Res. Annu.*4-7, 2002.
16. Yang, S. and Reitz, R.D., "A Continuous Multicomponent Fuel Flame Propagation and Chemical Kinetics Model," *Internal Combustion Engines* 132(7):072802, 2010, doi:10.1115/1.4000267.
17. Liang, L., Reitz, R.D., Iyer, C.O., and Yi, J., "Modeling Knock in Spark-Ignition Engines Using a G-equation Combustion Model Incorporating Detailed Chemical Kinetics," SAE Technical Paper 2007-01-0165, 2007, doi:10.4271/2007-01-0165.
18. Long, L., "*Multidimensional Modeling of Combustion and Knock in Spark-Ignition Engines with Detailed Chemical Kinetics*," (University of Wsconsin-Madison, 2006).
19. Tamagna, D., Gentili, R., Ra, Y., and Reitz, R.D., "Multidimensional Simulation of the Influence of Fuel Mixture Composition and Injection Timing in Gasoline-Diesel Dual-Fuel Applications," SAE Technical Paper 2008-01-0031, 2008, doi:10.4271/2008-01-0031.
20. Smith G., Golden D., Frenklach M., Moriarty N. et al., "GRI-Mechanism 3.0," http://combustion.berkeley.edu/gri-mech/version30/text30.html.
21. n-Heptane, Detailed Mechanism, Version 3.1, https://combustion.llnl.gov/mechanisms/alkanes/n-heptane-detailed-mechanism-version-3, 2011.
22. Bahlouli, K., Saray, R.K., and Atikol, U., "Effect of Heat Transfer on the Reduction of the Detailed Chemical Kinetics Mechanism in a Homogeneous Charge Compression Ignition Combustion Engine," *Proceedings of the Institution of Mechanical Engineers, Part D: Journal of Automobile Engineering* 229(14):1969-1980, 2015, doi:10.1177/0954407015575236.
23. Sun, W., Chen, Z., Gou, X., Ju, Y. et al., "A Path Flux Analysis Method for the Reduction of Detailed Chemical Kinetic Mechanisms," *Combustion and Flame* 157(7):1298-1307.
24. Sun, W., Chen, Z., Gou, X., and Ju, Y., "A Path Flux Analysis Method for the Reduction of Detailed Chemical Kinetic Mechanisms," *Combustion and Flame* 157(7):1298-1307, 2010, doi:10.1016/j.combustflame.2010.03.006.
25. Gao, X., Yang, S., and Sun, W., "A Global Pathway Selection Algorithm for the Reduction of Detailed Chemical Kinetic Mechanisms," *Combustion and Flame* 167:238-247, 2016, doi:10.1016/j.combustflame.2016.02.007.
26. Wang, P. and Bai, X.S., "Large Eddy Simulation of Turbulent Premixed Flames Using Level-Set G-Equation," *Proceedings of the Combustion Institute* 30:583-591, 2005, doi:10.1016/j.proci.2004.08.218.
27. Zha, K., Yu, X., Lai, M.-C., and Jansons, M., "Investigation of Low Temperature Combustion in an Optical Engine Fueled with Low Cetane Sasol JP-8 Fuel Using OH-PLIF and HCHO Chemiluminescence Imaging," SAE Technical Paper 2013-01-0898, 2013, doi:10.4271/2013-01-0898.

Nomenclature

ϕ - Equivalence Ratio

λ - Air -Fuel Equivalence Ratio

aTDC - after Top Dead Center

bTDC - before Top Dead Center

BMEP - Break Mean Effective Pressure
CAD - Crank Angle Degree
CI - Compression Ignited
CFD - Computational Fluid Dynamics
CO - Carbon Monoxide
CNG - Compressed Natural Gas
DRGEP - Direct Relation Graph with Error Propagation
IMEP - Indicated Mean Effective Pressure
RANS - Raynolds Averaged Navier Stokes
LLNL - Lawrence Livermore National Laboratory
PFA - Path Fux Analysis
PREMIER - PREmixed Mixture Ignition in the End-gas Region
SOI - Start of Injection

ISSN 0148-7191